ACS APPLIED MATERIALS & INTERFACES

Research Article

www.acsami.org

Magnetic Silica Nanotubes: Synthesis, Drug Release, and Feasibility for Magnetic Hyperthermia

Xuecheng Chen,*[,†] Rüdiger Klingeler,[‡] Matthias Kath,[‡] Ahmed A. El Gendy,[‡,§] Krzysztof Cendrowski,[†] Ryszard J. Kalenczuk,[†] and Ewa Borowiak-Palen[†]

[†]Institute of Chemical and Environment Engineering, West Pomeranian University of Technology, ul. Pulaskiego 10, 70-322, Szczecin, Poland

[‡]Kirchhoff Institute for Physics, Im Neuenheimer Feld 227, D-69120 Heidelberg, Germany

ABSTRACT: A new kind of silica nanotube with incorporated γ-Fe_2O_3 nanoparticles has been successfully prepared through sol−gel processes. Hematite particles supported on carbon nanotubes served as templates for the fabrication of the magnetic silica nanotubes. The obtained nanostructures consisting of magnetic Fe_2O_3 nanoparticles protected by a silica shell were fully characterized by transmission electron microscopy (TEM), X-ray diffraction (XRD), N_2 sorption and desorption, and magnetization studies. The hollow inner space and the magnetic functionalization render the material promising for applications in biology and medicine. This is underlined by studies in alternating magnetic fields which show a significant heating effect, i.e., the feasibility for applications in hyperthermia therapies. In addition, the material exhibits enhanced drug-loading capacity which is demonstrated by loading with rhodamine B molecules as drugs and corresponding release experiments. The results show that magnetic silica nanotubes can be straightforwardly synthesized and have a great potential as a multifunctional drug carrier system.

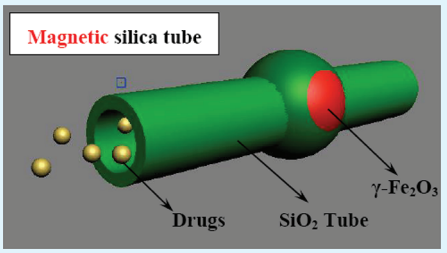

KEYWORDS: *silica tube, magnetic, carbon nanotube, heating effect, hyperthermia therapies, drug delivery*

INTRODUCTION

Silica-based nanomaterials attract much attention because of their nontoxic nature, tunable particle size and specific surface area, abundant Si−OH bonds on the particle surface, chemical/thermal stability, high drug loading capability, and sustained drug release from the supports.[1] Being a tubular nanomaterial, silica nanotubes exhibit empty inner space which can be filled by functional loads. In addition, the surface is hydrophilic and biocompatible so that the material can be applied in bioseparation, biocatalysis, biosensoring, and as drug/gene delivery carriers.[2] Hitherto, silica nanotubes have been typically fabricated in various templates,[3] using a surfactant-mediated sol−gel method[4] and a thermal oxidation-etching approach to convert the silicon nanowires into silica nanotubes.[5] Though silica nanotubes with different thickness and dimensions have been fabricated by changing the reaction parameters, the control and design of the wall structure remain contentious but desirable.[6] In addition to the mere properties of pristine silica tubes, adding magnetic functionality will be beneficial for applications in biology and medicine. To be specific, magnetic nanomaterials may be visualized by means of magnetic imaging modalities and/or serve as local probes for external magnetic fields. Hence, drug targeting by means of external magnetic gradient fields or local heating, i.e., magnetically induced hyperthermia, by means of alternating magnetic fields may be envisaged.[7,8] Thus, the combination of silica materials with magnetic particles is of great fundamental interest for, e.g., so-called "nanomedical" applications or liquid separation because of their high surface area and magnetic separability.[9]

In general, magnetic nanoparticles have been widely used in different fields, including advanced technological areas and biology. This field of biomagnetics is rapidly growing and consists of a broad range of current applications, including labeling and sorting of cells,[10] cell separation,[11] separation of biochemical products,[12] biosensing,[13,14] and studies of cellular function,[15] as well as a variety of other potential medical and therapeutic applications.[16] For biomedical applications, iron oxides are commonly used, i.e., maghemite (γ-Fe_2O_3) and magnetite (Fe_3O_4), due to enhanced biocompatibility with respect to other ferromagnetic materials. Nevertheless, the reactivity of iron oxide nanoparticles has been shown to greatly increase as their dimensions are reduced, and particles with relatively small size may undergo rapid biodegradation when they are directly exposed to biological environments.[17] Therefore, a suitable coating is essential to overcome such limitations, and encapsulation with silica endows the nanomagnets with several beneficial properties for their use in biomedical applications. Main parameters in this respect are compatibility in biological systems,[18] functionality, high colloidal stability under different conditions, the ability to modulate the magnetic properties with heating, and hydrophilicity.[19] Previous studies on composite nanomaterials consisting of iron oxide cores and silica shells indeed show promising magnetic properties, low cytotoxicity, chemically

Received: March 15, 2012
Accepted: April 9, 2012
Published: April 9, 2012

modifiable surfaces, applicability in bioseparation,[20] enzyme immobilization,[21] and diagnostic analysis.[22]

Surface functionalization is another relevant aspect of silica-based nanocomposites. Surface silanol groups can easily react with alcohols and silane coupling agents, not only to produce stable dispersions in nonaqueous solvents but also to provide ideal anchorage for the covalent binding of specific ligands. In particular, in the field of biomedical applications, covalent bonding of specific ligands such as, e.g., streptadivin or antibodies is facilitated which may enable binding to various targets such as cells, proteins, and nucleic acids or will allow antibody–antigen recognition.

Here, we present a novel and facile method to synthesize magnetic silica tubes with Fe_2O_3 nanoparticles inside the nanotubes. Through a template and sol–gel process, α-Fe_2O_3 nanoparticles first were deposited on carbon nanotubes. Subsequent silica coating and removal of the carbon nanotube template yields the magnetic silica tubes. The potential of this material for actual medical applications is demonstrated by drug loading and a related release study. In addition, the magnetic properties are investigated and the feasibility for magnetic hyperthermia is shown.

EXPERIMENTAL SECTION

Materials. Carbon nanotubes were bought from Shenzhen Nanoport Co., LTD, China (diameter: 20–40 nm). TEOS (95%), rhodamine B, and $FeCl_3$ were obtained from Sigma-Aldrich, which were used directly without further purification. All other materials were of analytical grade and commercially available, including $NH_3 \cdot H_2O$ (25% [w/w]) and ethanol.

Functionalization of Carbon Nanotubes. One gram of carbon nanotubes (as received) was suspended in 100 mL of concentrated nitric acid (65 wt %) and refluxed at 130 °C in an oil bath for 6 h. After the mixture was cooled down to room temperature, it was filtered through a polytetrafluoroethylene (PTFE) film with a pore diameter of 0.2 μm and washed with deionized water until the pH value of the filtrate was around 7. Then, the product was dried at 100 °C.

Fe_2O_3–CNT@SiO_2. In a typical synthesis procedure, the hexahedral hematite particle decorated carbon nanotubes were obtained via refluxing 60 mL of 2.0×10^{-2} M $FeCl_3$ aqueous solution with 50 mg of the above functionalized carbon nanotubes at 100 °C K for 24 h. After this process, the resultant hematite particle decorated carbon nanotubes were added to a solution of 1.7 mL of aqueous ammonia and 5.5 mL of water in *n*-propanol under stirring at room temperature for 30 min. Then, 0.6 mL of TEOS was rapidly added and continuously aged at room temperature for 24 h. The resultant mixture was filtrated and dried.

Magnetic γ-Fe_2O_3@SiO_2 Tubes. The dried sample was calcinated at 800 °C in Ar for 8 h to reduce the Fe_2O_3 to Fe_3O_4. The magnetic silica tubes were finally obtained by thermal treatment of the magnetic core/shell silica coated carbon nanotubes in air at 650 °C for 24 h; after this heating process, carbon nanotubes were completely burnt off.

Loading of Rhodamine B in γ-Fe_2O_3@SiO_2 Nanotubes (RhB@γ-Fe_2O_3@SiO_2). 50 mg of magnetic silica tubes were dispersed in a 30 mg/20 mL ethanol RhB solution, sonicated for 8 h, and then stirred for 48 h. After that, the sample was filtrated and dried under vacuum at 100 °C for 24 h.

Release Study. A typical drug release experiment was performed as follows: 37 mg of RhB@γ-Fe_2O_3@SiO_2 was immersed into 20 mL of phosphate-buffered saline (PBS, pH = 7.4) under magnetic stirring at a rate of ca. 100 rpm at room temperature. After removal of RhB@γ-Fe_2O_3@SiO_2 by magnet, 3 mL of the clear solution was extracted with a syringe at given time intervals and then analyzed by UV–vis spectroscopy at a wavelength of 400–1000 nm.

Characterization of Structure, Morphology, and Surface. X-ray diffraction (XRD) was conducted on a Philips diffractometer using Cu Kα radiation. Transmission electron microscopy (TEM) and high-resolution transmission electron microscopy (HR-TEM) were performed on a FEI Tecnai F30 transmission electron microscope with a field emission gun operating at 200 kV. The N_2 adsorption/desorption isotherms were acquired at liquid nitrogen temperature (77 K) using a Micromeritics ASAP 2010 M instrument, and the specific surface area was calculated by the Brunauer–Emmett–Teller (BET) method. The pore size distribution was determined using the Barret–Joner–Halenda (BJH) method.

Magnetic Studies. A MicroMag Model 2900 (Princeton Measurement Corp.) alternating gradient magnetometer (AGM) was applied for magnetization studies. The effect of AC magnetic fields was studied by means of a home-built setup consisting of a high frequency generator with a water cooled magnetic coil system at a frequency of 120 kHz, magnetic field strengths of 0–100 kA/m, and a fiber-optical thermometer.[23]

RESULTS AND DISCUSSION

Synthesis and Characterization. A synthesis scheme of magnetic silica nanotubes is shown in Figure 1. First,

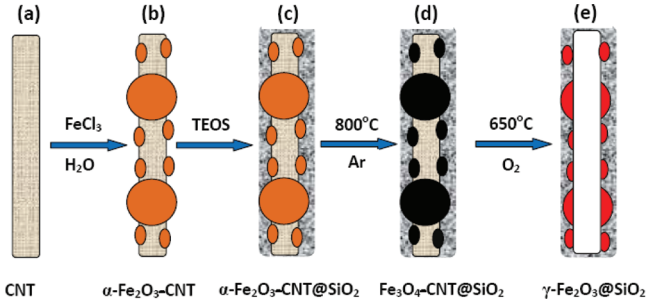

Figure 1. Schematic illustration of the synthesis of the magnetic silica nanotubes. From the left, (a) carbon nanotube serving as template, (b) deposition of hematite nanoparticles, (c) coverage by silica, (d) reduction of hematite to magnetite, and (e) removal of the carbon nanotube template by calcinations and concomitant oxidation of iron oxide (see the text).

functionalized carbon nanotubes (see Experimental Section) were exposed to $FeCl_3$ solution which hydrolyzed into β-FeOOH in water at 110 °C and then β-FeOOH transformed to α-Fe_2O_3. After this procedure, two kinds of uniform nanoparticles (β-FeOOH and α-Fe_2O_3) are present on the surfaces of the carbon nanotube templates (cf. Figure 1a,b). The small ones are α-Fe_2O_3 and the large ones are β-FeOOH. Thereafter, a silica layer with a desired thickness was deposited on the surface of the hematite core and carbon nanotubes by simultaneous sol–gel polymerization of tetraethoxysilane (TEOS) (Figure 1c). The hematite–CNT–silica composite was then heated in Ar at 800 °C in order to reduce the hematite nanoparticles to magnetite (Fe_3O_4). In the last step, magnetic silica nanotubes were finally obtained through removal of the carbon nanotube template by calcinations in air. Concomitantly, Fe_3O_4 is oxidized to γ-Fe_2O_3.

The procedure is visualized by TEM images of the intermediate and final products in Figure 2. Figures in the first row (Figure 2a–c) display α-Fe_2O_3-decorated carbon nanotubes. Noteworthy, the procedure yields two kinds of magnetic nanoparticles, i.e., with larger diameter of about 130 nm and smaller diameter of around 5 nm. High-resolution TEM images of either kind of particles are shown in Figure 2b,c. This size distribution is resembled by the Fe_2O_3 nanoparticle distribution in the final material which will be presented below in Figure 4. Images in Figure 2d–f show the

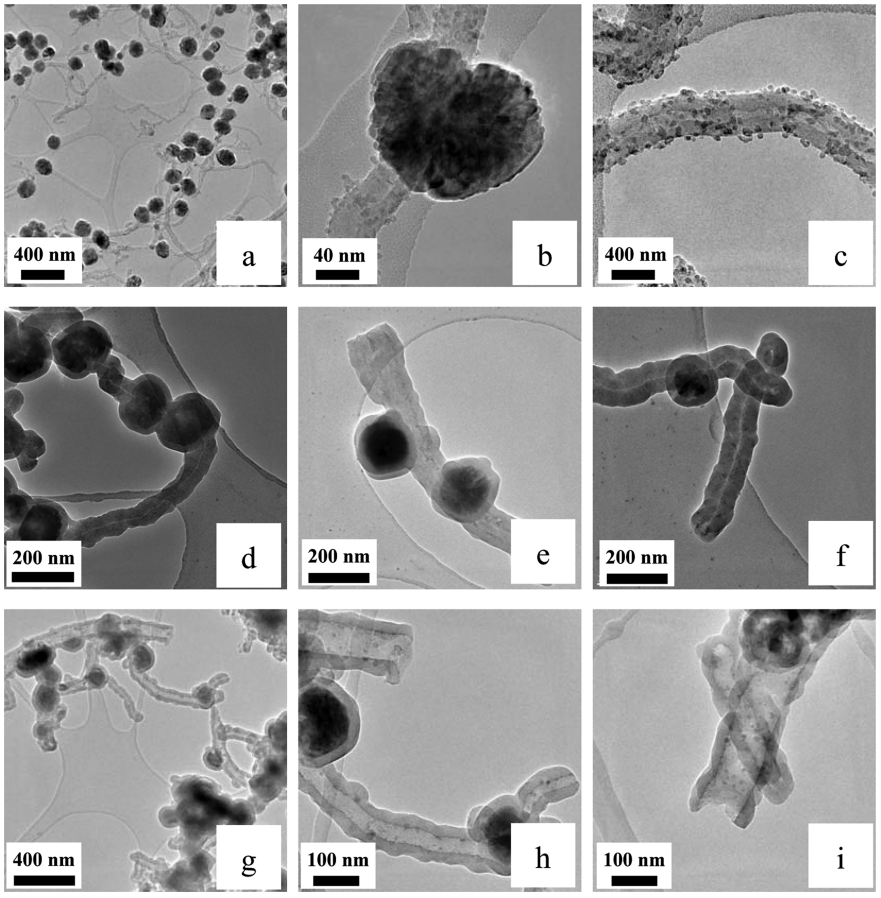

Figure 2. Illustration of the synthesis of magnetic silica nanotubes by TEM images. (a–c) Carbon nanotubes decorated with α-Fe_2O_3 nanoparticles; (d–f) silica coated α-Fe_2O_3–CNT nanocomposite; (g–i) magnetic silica nanotubes.

material after silica deposition (cf. Figure 1c). The TEM images clearly show that as well all carbon surfaces as the Fe_2O_3-nanoparticles are coated by the silica layer. Transformation of α-Fe_2O_3 to Fe_3O_4 occurs upon heating in Ar for 8 h in the presence of carbon. Subsequent high temperature heat treatment in air removes all carbon species which is displayed by the TEM images in Figure 2g–i. The data imply that carbon nanotubes have been completely removed leaving behind magnetically functionalized silica nanotubes. Big black spheres and small dots in Figure2h,i are attributed to γ-Fe_2O_3 nanoparticles. The TEM images show two kinds of differently sized Fe_2O_3 nanoparticles (cf. black dots and bigger nanoparticles in Figure 2b,c) distributed inside of the silica tubes. The silica tubes exhibit open ends through which additional load can be filled (released) into (out of) the hollow inner of the tubes as will be demonstrated by the drug filling and release experiment presented below.

In order to investigate the properties of the iron oxide nanoparticles, XRD studies have been performed on the final material as well as on the composite materials obtained during the intermediate synthesis steps explained above, i.e., α-Fe_2O_3–CNTs (cf. Figure 1b), silica coated α-Fe_2O_3–CNTs (cf. Figure 1c), (Fe_3O_4–CNTs)@SiO_2 (cf. Figure 1d), and Fe_2O_3@SiO_2 (cf. Figure 1e). Respective XRD patterns are displayed in Figure 3. All intermediate products which are supposed to contain carbon indeed show an intense peak at 2θ = 26° (marked by ∗) and broad ones at 42.7°(2θ) and 43.9°(2θ) corresponding to the characteristic [002] and [100] diffraction peaks of carbon nanotubes (JCPDS 65-6212), respectively.

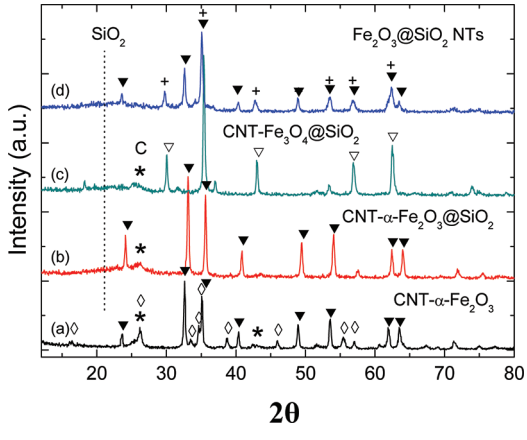

Figure 3. X-ray diffraction patterns of magnetic γ-Fe_2O_3@SiO_2 nanotubes (d) and of the materials obtained during the intermediate synthesis steps, i.e., α-Fe_2O_3–CNTs (a), silica coated α-Fe_2O_3–CNTs (α-Fe_2O_3–CNTs@SiO_2) (b), and (Fe_3O_4–CNTs)@SiO_2 (c). The peaks marked by the asterisk signal the presence of CNTs; ▽, ▼, ◊, and + mark diffraction peaks associated with the iron oxide phases (see the text). A broad hump at $2\theta \sim 22°$ indicates the presence of silica.

Pattern (a) is observed for the material where carbon nanotubes are covered with Fe_2O_3, i.e., it refers to the TEM images in Figure 2a–c. The observed peaks (marked by filled triangles) match the standard spectra of α-Fe_2O_3 (JCPDS No. 72-00469) so that indeed the α-Fe_2O_3–CNT composite is confirmed. In addition to α-Fe_2O_3, the XRD spectrum reveals

dx.doi.org/10.1021/am300469r | ACS Appl. Mater. Interfaces 2012, 4, 2303–2309

β-FeOOH (marked by ◊) which was applied in the first synthesis step. SiO_2-coating does not cause significant changes of the spectrum as seen in pattern (b) except for a broad peak around 22°(2θ), which is ascribed to silica, and the disappearance of the β-FeOOH phase. A new iron oxide phase however appears after heat treatment in Ar [pattern (c)] as indicated by diffraction peaks at 2θ = 30, 35.3, 43, 56, and 62° which prove the formation of Fe_3O_4 (open triangles). Finally, after calcination in air [pattern (d)], the signature of carbon nanotubes disappears while γ-Fe_2O_3 (+) and α-Fe_2O_3 (▼) is found and the signature of SiO_2 is still visible. Note, that magnetization data (not shown) confirm the XRD results since they do not show any indication of the transition typically appearing in magnetite but exhibit a broad feature which may be associated with the Morin transition in hematite nanoparticles.

Interestingly, there is an unusual size distribution of the magnetic nanoparticles in the final material as presented in Figure 4. Similar to the findings in Figure 2b,c where the

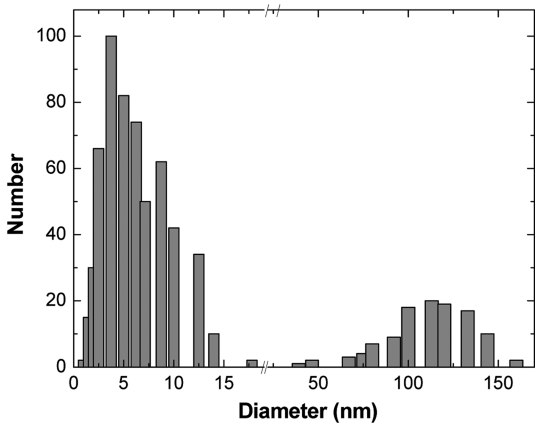

Figure 4. Diameter distribution of γ-Fe_2O_3 nanoparticles inside the silica nanotubes.

initially decorated particles separate in portions of either small (~5 nm) or large (~130 nm) particles, a similar distribution is observed for Fe_2O_3 particles in the final composite material. Analysis of the XRD peaks by means of the Scherrer equation,[24] which exploits the peak width for analysis of the mean particle size, does not yield clear differences between the mean size of hematite and maghemite particles. In both cases, the Scherrer analysis yields mean XRD-particle diameters of 20−30 nm (which in this case of well separated portions of differently sized particles is however not a meaningful quantity). We note that differently sized magnetic particles exhibit different functionalities. In general, small particles are beneficial when aiming at magnetic hyperthermia while larger particles are needed if an external magnetic field gradient shall exert force for moving the particle.

For further characterization of the material, we studied the specific surface area and the pore size distribution. The nitrogen adsorption/desorption isotherm (Figure 5) indicates a linear increase in the amount of adsorbed nitrogen in a high relative pressure. The isotherm represents a behavior typical for relatively large pore (type IV, H1) curves, characteristic of a mesoporous (2−50 nm pore diameter) material, with a sharp up turn in the high relative pressure region.[25] The steep increase in adsorbed nitrogen at relative pressures between 0.8 and 1.0 P/P_0 reflects a narrow pore size distribution, which also

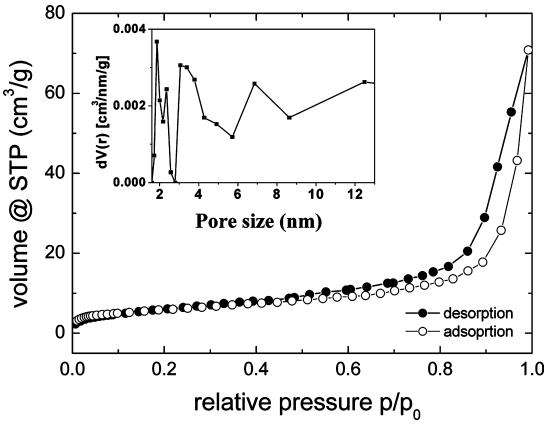

Figure 5. N_2 adsorption isotherms and corresponding pore size distribution curve of MSNTs and corresponding pore diameter distribution.

can be seen from the inset curve in Figure 5. Quantitatively, analyzing the adsorption branch of the nitrogen isotherm by means of the BJH method yields pore diameters of 1.8, 2.3, 3, 6.8, and 12 nm (inset of Figure 5). Note, that the small values have to be taken with care since the analysis is limited to pore sizes D_P > 2 nm. and due to the restriction to the pressure regime P/P_0 > 0.42, the results with D_P < 4 nm have to be assessed critically.[26] The BET surface area and the BJH desorption cumulative volume of pores of the magnetic silica tubes are 20.4 m^2/g and 0.105 cm^3/g, respectively.

Magnetic Properties. The field dependence of the magnetization M(B) of the γ-Fe_2O_3@SiO_2 powder sample, i.e., the full hysteresis loop of the magnetization, in external fields up to 1T is presented in Figure 6. The data reveal a

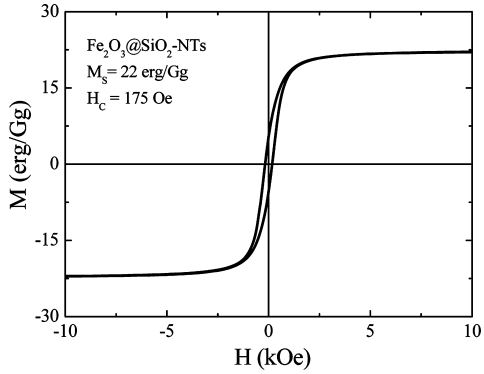

Figure 6. Magnetization of Fe_2O_3@SiO_2 nanotubes at T = 300 K.

ferromagnetic behavior at room temperature which corresponds to the fact that most of the magnetic material is not in the superparamagnetic limit. To be more specific, although Figure 4 reveals much more smaller (i.e., d < 20 nm) than larger particles, the former only comprise ~0.2% of the ferrimagnetic material. Note, that according to the parameters in ref 27 only particles with diameter below ~10 nm are superparamagnetic at 300 K. Quantitatively, the saturation magnetization, the remanent magnetization, and the coercivity amount to M_S = (22 ± 2) erg/Gg, M_R = (5.5 ± 2) erg/Gg, and H_C = (175 ± 4) Oe, respectively. Neglecting the magnetic response of hematite, which at room temperature is 2 orders of magnitude smaller than that of maghemite, allows one to extract the relative maghemite content in the composite

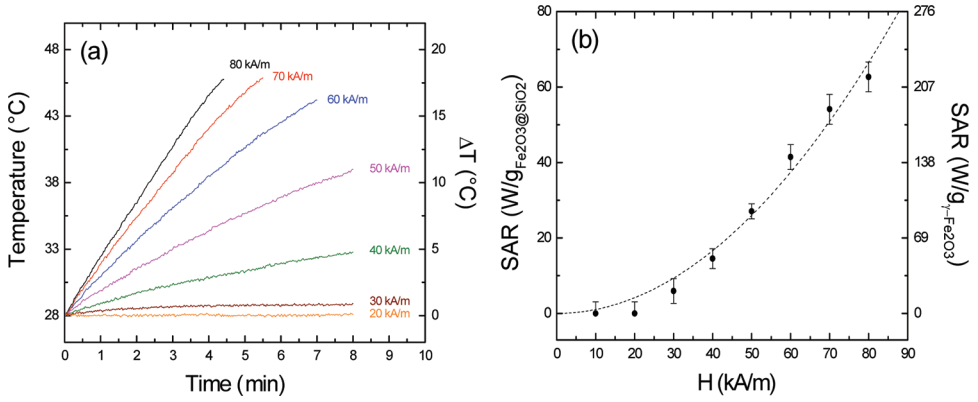

Figure 7. (a) Temperature vs time upon application of AC magnetic fields at various field strengths and a frequency of f = 120 kHz and (b) corresponding SAR values for the γ-Fe_2O_3@SiO_2 tubes.

material. Comparison with the corresponding data of maghemite bulk material (M_S = 76 erg/Gg at 300 K)[28] hence enables one to infer that ~29 wt % maghemite is present in the material. We note that the saturation magnetization decreases upon size reduction in γ-Fe_2O_3[29] so that the actual maghemite content might be slightly larger.

The feasibility of the γ-Fe_2O_3@SiO_2 nanocomposite for magnetically induced heating has been investigated by measuring dissipation effects under applied AC magnetic fields. In particular, the temperature dependence $T(t)$ was studied under applied AC magnetic fields with a fixed frequency of 120 kHz and various magnetic field strengths of up to 80 kA/m. The temperature of the sample was measured by a fiber-optical temperature sensor.[30,31] This measurement was carried out for a dispersed sample in aqueous solution. In order to get the dispersion, carboxy methyl cellulose (CMC) has been used as a biocompatible surfactant. The particles were dispersed in a water−CMC solution using a tip sonicator for 2 min (10 s on and 1 s off, respectively). The concentration of the particles as well as of CMC in the water was approximately 5 mg/mL.

In Figure 7a, the time-dependent calorimetric measurements at different applied magnetic field strengths for γ-Fe_2O_3@SiO_2 are shown. A heating effect has been observed at applied magnetic fields >20 kA/m. The heating rate reached values of 4 °C/min at the maximum applied magnetic field of 80 kA/m. The heating ability of the sample in the solution is usually displayed via the specific absorption rate (SAR) which reflects the feasibility of a material for application in magnetic hyperthermia therapy. The SAR values shown in Figure 7b have been calculated from the initial slope of the T versus t curves. The observed roughly quadratic field dependence is in agreement with the fact that the dissipated magnetic energy is proportional to H^2. SAR is however rather moderate. For example, at 50 kA/m, we find SAR ~ 27 W/g, i.e., SAR ~ 90 $W/g_{\gamma\text{-}Fe2O3}$. Assuming a quadratic field dependence, our data hence suggest that SAR (H = 5 kA/m) is less than 1 $W/g_{\gamma\text{-}Fe2O3}$ which is by a factor of about 30 smaller than that found for superparamagnetic SiO_2-coated γ-Fe_2O_3 by Yu et al.[32] This difference is associated with the fact that the magnetic core particles in ref 30 exhibit diameters of about 20 nm while most of the maghemite particles at hand are significantly larger (cf. Figure 4) so that Neel-type of dissipation effects are strongly reduced.

Zeta sizer measurements were done in order to determine the state of aggregation of magnetic silica tube suspensions. As shown in Figure 8, there were two peaks appearing, centered at

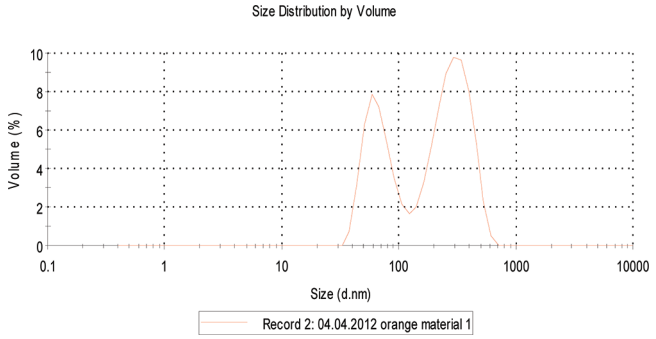

Figure 8. Size distribution of magnetic silica tubes.

76 and 286 nm, which means that the magnetic silica tubes can be used for biomedical applications.

Drug Release Experiments. The open-ended nanotubular structure renders the present magnetic silica tubes potentially applicable in drug delivery. This feasibility for carrying a significant drug load and slow release of the therapeutic material is demonstrated by the results in Figure 9. Here, rhodamine B was used as drug molecule to be stored and released from the magnetic silica tubes. Figure 9a shows UV−vis spectra of the aqueous media in which rhodamine B was released from RhB@γ-Fe_2O_3@SiO_2 for a given time after respective removal of the γ-Fe_2O_3@SiO_2 carrier. The broad absorption band around 553 nm is characteristic for RhB so that its intensity allows estimating the RhB concentration in the solution. The data indeed confirm drug loading and release since the rhodamine B concentration gradually increases with time, indicating sustained release of rhodamine B molecules. In the first 5 h release, nearly 50% of RhB was released from the γ-Fe_2O_3@SiO_2 tube. The kinetics of the process can be inferred from Figure 9b which implies that about 80% of the RhB load is released from RhB@γ-Fe_2O_3@SiO_2 within 9 h. The total RhB storage capacity in the γ-Fe_2O_3@SiO_2 tube is 9.25 mg/g. Because of the large open ends and the results from pore diameter distribution, the magnetic nanotubes are also favorable for loading big sized drug molecules; further investigations such as introducing DNA or RNA into the magnetic nanotubes will be done in the future.

CONCLUSIONS

In summary, we present a straightforward synthesis method for magnetically functionalized silica nanotubes. The method employs carbon nanotube templates and can be easily upscaled

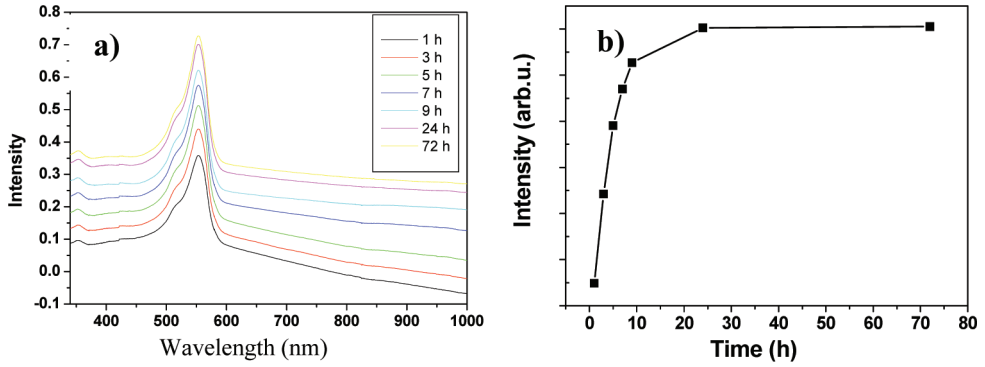

Figure 9. Time-dependent release of rhodamine B from magnetic silica tubes in PBS solution. Time dependence of (a) UV−vis spectra and (b) intensity of the characteristic for RhB absorption band.

in order to achieve economic and fast production of the material. The material exhibits a considerable magnetization and has a hollow structure which suggests applications with multifunctional character. Our experiments indeed show that local heating is induced by applied alternating magnetic fields which shows the materials' potential for magnetic hyperthermia therapies. In addition, we show that it can serve as a drug carrier system since a significant amount of rhodamine B was loaded to the material and its release was studied. Interestingly, encapsulated magnetic nanoparticles divide into two differently sized portions, i.e., into particles in the 10 nm and in the 100−200 nm range, respectively. This behavior may be exploited for different magnetic functions since small particles are beneficial when aiming at magnetic hyperthermia while larger particles are needed if an external magnetic field gradient shall exert force for moving the particle.

AUTHOR INFORMATION

Corresponding Author

*E-mail: xchen@zut.edu.pl.

Present Address

[§]National Institute for Standards, Giza, P.O. Box 12211, Giza, Egypt.

Notes

The authors declare no competing financial interest.

ACKNOWLEDGMENTS

The work was supported by Foundation for Polish Science within Focus with contract F4/2010.

REFERENCES

(1) (a) Vallet0cas-Regi, M.; Rámila, A.; del Real, R. P.; Pérez-Pariente, J. *Chem. Mater.* **2001**, *13*, 308. (b) Munoz, B.; Ramila, A.; Pariente, J. P.; Diaz, I.; Vallet-Regi, M. *Chem. Mater.* **2003**, *15*, 500. (c) Horcajada, P.; Ramila, A.; Pariente, J. P.; Vallet-Regi, M. *Microporous Mesoporous Mater.* **2004**, *68*, 105. (d) Zhu, Y.; Shi, J.; Shen, W.; Dong, X.; Feng, J.; Ruan, M.; Li, Y. *Angew. Chem., Int. Ed.* **2005**, *44*, 5083.

(2) Llusar, M.; Sanchez, C. *Chem. Mater.* **2008**, *20*, 782.

(3) Hillebrenner, H.; Buyukserin, F.; Kang, M.; Mota, M. O.; Steward, J. D.; Martin, C. R. *J. Am. Chem. Soc.* **2006**, *128*, 4236.

(4) Jang, J.; Yoon, H. *Adv. Mater.* **2004**, *16*, 799.

(5) Fan, R.; Wu, Y.; Li, D.; Yue, M.; Majumdar, A.; Yang, P. *J. Am. Chem. Soc.* **2003**, *125*, 5254.

(6) Yang, Y. K.; Qiu, S. Q.; Cui, W.; Zhao, Q.; Cheng, X. J.; Li, R. K. Y.; Xie, X. L.; Mai., Y. W. *J. Mater. Sci.* **2009**, *44*, 4539.

(7) Pankhurst, Q. A.; Conolly, J.; Jones, S. K.; Dobson, J. *J. Phys. D: Appl. Phys.* **2003**, *36*, 167.

(8) Klingeler, R.; Hampel, S.; Büchner, B. *Int. J. Hyperthermia* **2008**, *24*, 496.

(9) (a) Bourlinos, A. B.; Simopoulos, A.; Boukos, N.; Petridis, D. *J. Phys. Chem. B* **2001**, *105*, 7432. (b) Coradin, T.; Larionova, J.; Smith, A. A.; Rogez, G.; Clerac, R.; Guerin, C.; Blondin, G.; Wimpenny, R. E. P.; Sanchez, C.; Mallah, T. *Adv. Mater.* **2002**, *14*, 896. (c) Wu, P.; Zhu, J.; Xu, Z. *Adv. Funct. Mater.* **2004**, *14*, 345. (d) Giri, S.; Trewyn, B. G.; Lin, V. S. Y. *Angew. Chem., Int. Ed.* **2005**, *44*, 5038. (e) Sen, T.; Sebastianelli, A.; Bruce, L. J. *J. Am. Chem. Soc.* **2006**, *128*, 7130. (f) Dong, X.; Chen, H.; Zhao, W.; Li, X.; Shi, J. *Chem. Mater.* **2007**, *19*, 3484.

(10) Chemla, Y. R.; Crossman, H. L.; Poon, Y.; McDermott, R.; Stevens, R.; Alper, M. D.; Clarke, J. *Proc. Natl. Acad. Sci. U.S.A.* **2000**, *97*, 14268.

(11) (a) Bergemann, C.; Muller-Schulte, D.; Oster, J.; Brassard, L. A.; Lubbe, A. S. *J. Magn. Magn. Mater.* **1999**, *194*, 45. (b) Rudiger, K.; Larsen, F.; Jakobsen, K. S. *Appl. Environ. Microbiol.* **1998**, *64*, 34.

(12) Ugelstad, J.; Berge, A.; Ellingsen, T.; Schmid, R.; Nilsen, T.-N.; Mork, P. C.; Stenstad, P.; Hornes, E.; Olsvik, O. *Prog. Polym. Sci.* **1992**, *17*, 87.

(13) Baselt, D. R.; Lee, G. U.; Natesan, M.; Metzger, S. W.; Sheehan, P. E.; Colton, R. J. *Biosens. Bioelectron.* **1998**, *13*, 731.

(14) Vyalikh, A.; Wolter, A.; Hampel, S.; Haase, D.; Ritschel, M.; Leonhardt, A.; Grafe, H.-J.; Taylor, A.; Krämer, K.; Büchner, B.; Klingeler, R. *Nanomedicine* **2008**, *3*, 321.

(15) MacKintosh, F. C.; Schmidt, C. F. *Curr. Opin. Colloid Interface Sci.* **1999**, *4*, 300.

(16) (a) Pankhurst, Q. A.; Connolly, J.; Jones, S. K.; Dobson, J. *J. Phys. D: Appl. Phys.* **2003**, *36*, 167. (b) Tartaj, P.; Morales, M. P.; Veintemillas-Verdaguer, S.; González-Carreño, T.; Serna, C. J. *J. Phys. D: Appl. Phys.* **2003**, *36*, 182.

(17) Maceira, V. S.; Correa-Duarte, M. A.; Spasova, M.; Liz-Marzán, L. M.; Farle, M. *Adv. Funct. Mater.* **2006**, *16*, 509.

(18) Yoon, T.-J.; Kim, J. S.; Kim, B. G.; Yu, K. N.; Cho, M.-H.; Lee, J.-K. *Angew. Chem., Int. Ed.* **2005**, *44*, 1068.

(19) (a) Tartaj, P.; Serna, C. J. *J. Am. Chem. Soc.* **2003**, *125*, 15754. (b) Tartaj, P.; González-Carreño, T.; Serna, C. J. *Adv. Mater.* **2001**, *13*, 1620.

(20) Xu, X. Q.; Deng, C. H.; Gao, M. X.; Yu, W. J.; Yang, P. Y.; Zhang, X. M. *Adv. Mater.* **2006**, *18*, 3289.

(21) Li, Y.; Yan, B.; Deng, C. H.; Yu, W. J.; Xu, X. Q.; Yang, P. Y.; Zhang, X. M. *Proteomics* **2007**, *7*, 2330.

(22) Levy, L.; Sahoo, Y.; Kim, K.-S.; Bergey, E. J.; Prasad, P. N. *Chem. Mater.* **2002**, *14*, 3715.

(23) Krupskaya, Y.; Mahn, C.; Parameswaran, A.; Taylor, A.; Krämer, K.; Hampel, S.; Leonhardt, A.; Ritschel, M.; Büchner, B.; Klingeler, R. *JMMM* **2009**, *321*, 4067.

(24) Patterson, A. L. *Phys. Rev. Lett.* **1939**, *56*, 978−982.

(25) (a) Gregg, S. J.; Sing, K. S. W. *Adsorption, Surface Area and Porosity*, 2nd ed.; Academic: New York, 1982. (b) Webb, P. A.; Orr, C. *Analytical Methods in Fine Particle Technology*; Micromeritics Instrument Corp.: Norcross, GA, 1997.

(26) Sing, K. S. W.; Rouquerol, J. In *Handbook of Heterogenous Catalysis*; Ertl, G., Knözinger, H., Eds.; Wiley-VCH, Weinheim, 1997; Vol. 2.
(27) Nadeem, K. *J. Magn. Magn. Mater.* **2011**, *323*, 1998−2004.
(28) Berkowitz, A. E.; Shuele, W. J.; Flanders, P. J. *J. Appl. Phys.* **1968**, *39*, 1261.
(29) Lu, H. M. *J. Phys. D: Appl. Phys.* **2007**, *40*, 320−325.
(30) Krupskaya, Y.; Mahn, C.; Parameswaran, A.; Taylor, A.; Kraemer, K.; Hampel, S.; Leonhardt, A.; Ritschel, M.; Büchner, B.; Klingeler, R. *J. Magn. Magn. Mater.* **2009**, *321*, 4067.
(31) El-Gendy, A. A.; Ibrahim, E. M. M.; Khavrus, V. O.; Krupskaya, Y.; Hampel, S.; Leonhardt, A.; Büchner, B.; Klingeler, R. *Carbon* **2009**, *47*, 2821.
(32) Yu, J. H. *J. Mater. Sci. Technol.* **2010**, *26*, 333.